Applying high-resolution 3D CSEM and seismic for integrated reservoir characterization

John Reidar Granli, Daria Daudina, and Sarah Catherine Robertson, OMV Norway;*
Jan Petter Morten, Pål T. Gabrielsen, and Bård Sigvathsen, EMGS ASA

Summary

In this paper we describe the application of high-resolution 3D CSEM and seismic data for a shallow exploration target called Gemini N close to the Wisting discovery in the Barents Sea. Like Wisting, Gemini N also exhibits coincident CSEM and seismic anomalies that support the presence of high-saturation hydrocarbon reservoir, but the situations in the two data domains are still very different. Compared to Wisting, the seismic anomaly at Gemini N is much stronger, while the CSEM anomaly is much weaker. The shallow target burial depth combined with a high resistivity background was an ideal setting to deploy high-resolution CSEM. Feasibility modeling showed that CSEM frequencies as high as ~50 Hz with a 1 km receiver and 500 m towline spacing would be effective. A new acquisition led to results that were revealing and realized much higher resolution and sensitivity to the buried resistor properties. For seismic, a 3D ultra-high resolution (P-Cable) dataset was already available over Gemini N. These data provided vital details to the reservoir geometry and were very important for the joint seismic and CSEM interpretation of Gemini N. Our pre-drill prediction came out accurate for thickness of pay in good reservoir. There was still a caveat, though. Unlike Wisting this one was gas which is still a challenge in much of the Barents Sea.

Introduction

The Hoop area of the Barents Sea is an active exploration area, and several new concepts for 3D CSEM acquisition and imaging have been tested here. An important learning from the Wisting field appraisal is that CSEM data can provide high-resolution imaging in terms of outlining and predicting hydrocarbon reservoirs (Granli et al., 2017; Morten et al., 2017). In this paper, we investigate a nearby exploration target which has similar geological history and is situated in the same shallow reservoir level as Wisting. Our story is CSEM centric with a focus on integration of CSEM and seismic data during interpretation. The project work has been multi-disciplinary with sharing and learning as vital ingredients, and "questioning the given" is our mode of operation which means to always investigate explanations when anomalies in the data challenge established models.

At the outset of the area evaluation, the seismic database had conventional wide-tow 3D. Some adaptation to shallow targets was achieved by reprocessing with effective source and receiver de-ghosting to enhance resolution. The existing 3D CSEM survey data were acquired using a grid that was designed for regional exploration and had not been optimized for the target (3 km × 3 km receiver and 3 km towline spacing). Based on recent learning from Wisting, high frequencies up to 16 Hz had been used in inversion. As a reference to the database, the seismic and CSEM responses at Wisting and Gemini N are compared for Stø Fm level in Figure 1. The average resistivity estimate from CSEM was substantially weaker at Gemini N, while the seismic amplitude at the top reservoir was much stronger when compared to Wisting. But qualitatively, the area was anomalous in both data domains in the same way as Wisting. Based on the track record for Stø Fm targets in the Hoop area, the presence of a CSEM anomaly has been a reliable signature of hydrocarbon saturated reservoir, provided presence of seismic DHI. The very strong seismic amplitude does suggest a more gas prone setting, or perhaps oil in a different reservoir or Fuglen cap rock. The weaker CSEM response could indicate a thinner reservoir/pay, a complex resistor geometry, or poorer reservoir quality. The coarser acquisition grid was also understood to be a factor.

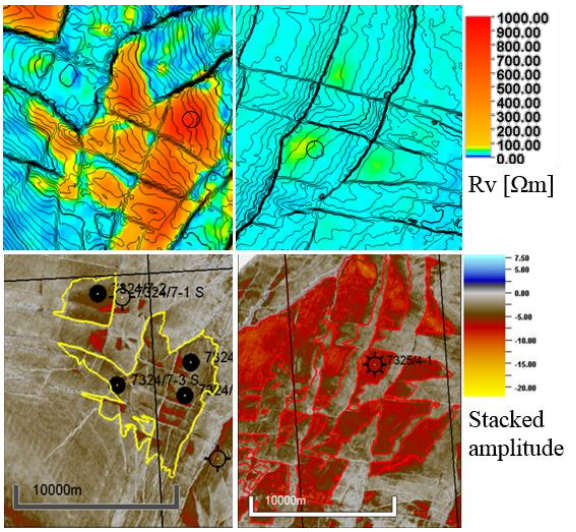

Figure 1 Comparing the response from 3D CSEM (top row) and seismic (bottom row) at Wisting (left column) and Gemini N (right column). The seismic shows the amplitude for a Stø reservoir, while the CSEM shows the average resistivity from inversion.

High-resolution 3D CSEM

Increasing the towline and receiver density and transmitter frequency has been shown to give a phenomenal improvement in resolution and sensitivity in this area. Could we take this further and zoom into a detailed mapping of the

10.1190/segam2018-2995351.1

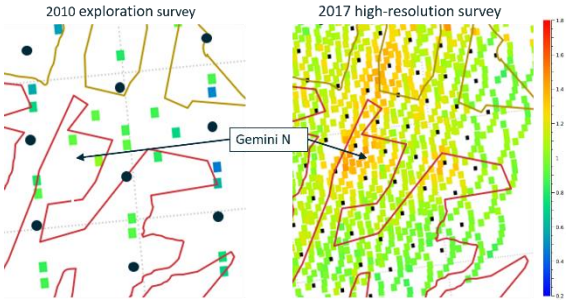

Figure 2 NMvO attribute $\left|E_i^{\text{Observed}}/E_i^{\text{Reference}}\right|$ from 3D CSEM, source-receiver offset 2.5 km, frequency 20 Hz. Left: Coarse-grid 2010. Right: High-resolution 2017. The same synthetic reference data was created by plane-layer modeling using homogeneous background resistivity. Black symbols show receiver positions.

Gemini N resistor, much different from the one shown in Figure 1 top right? That would require a new survey with optimized parameters. A survey design study was initiated. The objective was to determine whether denser spatial sampling and higher frequencies could image shallow targets with higher confidence and accuracy. Preliminary modeling determined that the peak sensitivity to Stø Fm targets with small area (< 5 km^2) and weak anomalous transverse resistance (ATR, see Morten et al., 2017) (< 1 kΩm^2) is at frequencies above 20 Hz and at source-receiver offsets below 4 km. A supporting illustration is shown in Figure 2 where the ~20 Hz normalized magnitude versus offset (NMvO) attribute from the vintage dataset is compared with data from the 2017 high-resolution survey at Gemini N. Note also the uneven target illumination using the vintage survey parameters which affects imaging and interpretation, especially for weak and small resistors.

Figure 3 summarizes results from a synthetic data inversion study with varying acquisition geometries and source frequencies. The water depth and background resistivity correspond to the measurements from the survey area. We introduced a reservoir with varying thickness and lateral distribution defined by seismic prospects. The reservoir resistivity is 600 Ωm. This corresponds to the Stø Fm resistivity at the irreducible water saturation according to an EM property rock physics model developed for this area. The background resistivity includes a high-resistive half-space at the Triassic level starting ~400 m below the reservoir. This resistive layer is important to include, as the imaging capability is challenged with smearing this layer and the reservoir response. The first test A in Figure 3 mimiced the existing data set with 3 km by 3 km receiver spacing and north-south source towing every 3 km. In addition, a few east-west lines are towed. The frequency range is 1 to 22 Hz. This spans propagation skin-depths of approximately 500 to 2000 m. Since the skin-depth is the shortest scale for signal propagation, this indicates a scale for imaging resolution. Hence, the depth uncertainty of the resistor placement can be estimated ≤500 m. The inversion results show that the thickest part of the reservoir is imaged as a "bump" on the high resistive Triassic layer, and is therefore ambiguous – the response could also be lithology related. The main aim of the survey optimization going forward was therefore to improve imaging resolution rather than target sensitivity. Note from the average resistivity map (Figure 3 left) that the imaging is achieved only along the source towlines where short source-receiver offsets (< 4 km) are available. Due to the 3 km receiver and towline spacing, available offsets for azimuthal data sensitive to some target in-between towlines will be from approximately 4 km.

A denser survey grid increases short-offset sampling. The effect is shown in Figure 3B where we consider 1 km by 1 km receiver spacing, and source towing every 0.5 km in the south-north direction. Here the source is towed above all receiver lines, and in-between each receiver line. The imaging confidence is improved dramatically. From the average resistivity map we can see that most of the thick parts of the reservoir are imaged, including some smaller compartments. Further increasing data sampling density only marginally improves the imaging (not shown).

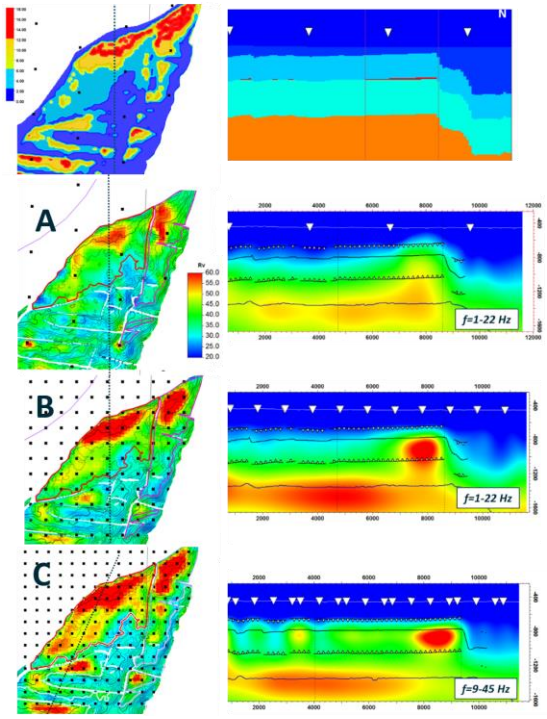

Figure 3. Synthetic study of acquisition configurations. Top: Reservoir net pay thickness map and S-N resistivity cross section. Below: Inversion results for different acquisition geometries and frequency ranges. (A) Receiver and towline spacing 3 km, 1-22 Hz (B) Receiver spacing 1 km, towline spacing 0.5 km, 1-22 Hz (C) Receiver spacing 0.75 km, towline spacing 0.375 km, 9-45 Hz.

10.1190/segam2018-2995351.1

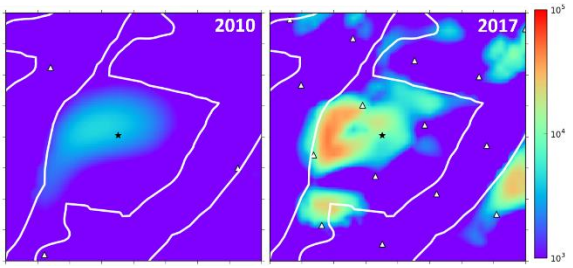

Figure 4 ATR (color scale) maps from constrained 3D CSEM inversion from the 2010 vintage data (left) and from the new 2017 high-resolution data (right). The black dot shows the position of the Gemini N well location, while the triangles show the corresponding CSEM receiver locations for the two surveys.

However, if we increase the frequency range to include frequencies up to 45 Hz with the same acquisition geometry, the effect on imaging is again dramatically improved as seen in Figure 3C. The average resistivity map shows a very good correlation to the original reservoir thickness map, capturing the small compartments. The vertical sections show an accurate depth placement of the target with well-defined separation from the resistive Triassic layer. This improvement in depth placement and separation is due to the decrease of skin-depth from 500 m (22 Hz) to 300 m (45 Hz).

The potential to improve imaging and hence interpretation of the weak Gemini N resistor motivated acquisition of a new high-resolution 3D CSEM survey. The receiver loggers were reconfigured for sampling of the waveform with a high 48 Hz signal component. The receiver grid was 1 km by 1 km, with source towlines every 500 m. The towing direction was changed from north-south to nortwest-southeast to cross most of the prospects perpendicular to their longest axis. When the target sensitivity is good, this orientation gives better imaging resolution. The high frequency f used in the survey puts strict requirements on receiver timing accuracy. The phase uncertainty $\delta\phi = 2\pi f\ \delta t$ scales with the high frequency and thus the timing error δt must be kept small for the entire receiver deployment. Requiring that $\phi < 5°$ to reliably resolve subsurface resistivity, we must have $\delta t <$ 0.3 ms. While processing the survey data, a procedure involving timing calibration-points at drop, recovery, and source overpass was employed. Detailed modeling of the near-field at source overpass combined with accurate timing from the vessel enabled the latter calibration.

Figure 4 summarizes the improvements achieved with the new high-resolution survey. It compares the ATR for the shallow target from the original vintage with 3 km spacing between receivers and towlines (2010) and the new high-resolution acquisition with 1 km between receivers and 0.5 km spacing between towlines (2017). The new data confirm the findings from the modeling study, with enhanced recovery and improved spatial resolution, even recovering internal resistor variations. The result also confirmed a clear separation between the lower Triassic and

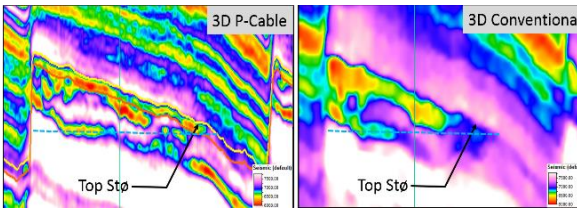

Figure 5. Comparing Gemini N acoustic impedance inversion results. Left: P-Cable, right: conventional data. Well location is shown as a vertical line, the estimated fluid contact by dashed line.

the reservoir intervals, as predicted (not shown). The ATR reconstruction using a seismic depth-constraint shows that resistor details on the 200 m scale are now resolved, which is compatible with the shortest scales of signal propagation. We used a rock physics model to relate ATR to hydrocarbon column height using well log calibration data for a good reservoir at Wisting. The prediction at the well location was ~11 m column, where the estimate depends on assumed reservoir quality.

Joint interpretation of seismic and CSEM

Seismic is our main tool for detailed interpretation of the subsurface. In the setting with the target reflection arriving before the first seabed multiple, the seismic quality has been exceptional. This is important for accurate integration with CSEM data. The better the seismic, the more precise are the structure constraints used to extract quantitative resistivity estimates from CSEM data. Still, and in spite of this connection, we choose to proceed with inversion of seismic and CSEM individually. The subsequent joint interpretation may require repeated inversions to obtain consistency. This "individual" inversion strategy is motivated by the fundamental difference between CSEM and seismic regarding length scale and parameter sensitivity. Also, an effective crosstalk between "acoustic and electric" domains in this case would be particularly difficult due to a very different parameter sensitivity across domains. Others seem to achieve interesting results from joint inversion, e.g. Alvarez et al. (2017) and Miotti et al. (2013).

A few seismic vintages exist in our study area and two of them are included in Figure 5 with P-Cable to the left and conventional 3D seismic data to the right. P-Cable is the trademark for an ultra-high resolution seismic technology described with more detail in Garden et al. (2017) and Moskvil et al. (2018). Both datasets have been 3D time migrated, stacked and inverted for acoustic impedance (AI). The X-section goes through the planned Gemini N well location with an E-W orientation. The P-Cable data resolution improvement is remarkable and provides a substantially more detailed and accurate representation of

10.1190/segam2018-2995351.1

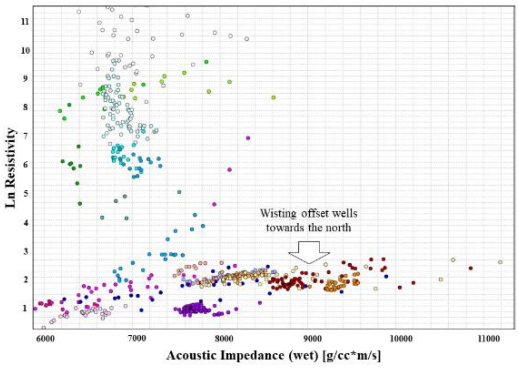

Figure 6. Distribution of in-situ ln resistivity (laterolog) vs acoustic impedance (fluid substituted to wet) for the Stø Fm. Only released wells in Hoop are included. The colors indicate facies.

reservoir geometry and property variations. Stø Fm is clearly not a thick uniform layer as anticipated but exhibits variation in acoustic impedance and hence also in reservoir properties. This corresponding variation is supported by our understanding of variability for the Stø Fm across the Hoop area, as illustrated by the Figure 6 cross-plot. The large range in acoustic impedance is largely driven by sedimentary facies variability of (indicated by the colors) and reservoir quality. In a regional sense the reservoir heterogeneity in the Stø Fm is increasing towards the north from Wisting. The layered impedance distribution estimated from P-Cable data at the well location (see Figure 5) may therefore be significant and suggested a slightly degraded reservoir quality in the upper compared to the lower Stø section at the upcoming well location. Alternatively, this could also imply a locally harder thin Stø over a softer Fruholmen. Such detailed AI based interpretation would not be possible based on the conventional inversion data, as shown in Figure 5. Note also that while the AI of wet Stø Fm reservoir spans a continuum for these wells, there is a separation along the resistivity axis exceeding a decade as a result of saturation.

In Figure 7 we compare the seismic P-Cable and high-resolution CSEM images over Gemini N. The seismic shows a windowed RMS distribution of AI within Stø Fm while the CSEM shows average resistivity from constrained inversion. Within the well segment there is a clear correspondence towards the south and west, between areas of low impedance above the gas water contact and high resistivity. There is also a clear and coinciding seismic and CSEM anomaly at the planned well location. There is still some way from a perfect match and we investigate if further alignment is possible.

Based on the P-Cable we may assume that the ~20 m Stø Fm is stratified into ~6 m upper high AI over ~12 m low AI. Due to the high sensitivity of resistivity to reservoir facies in saturated Stø Fm, it is likely that only the lower ~12 m with smaller AI and presumably better reservoir, will make significant contribution ATR estimated from the CSEM

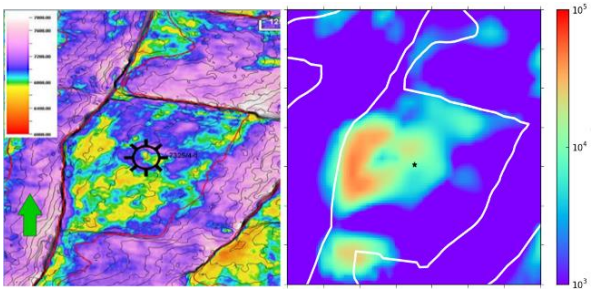

Figure 7. Comparing P-Cable (15 ms RMS AI inversion) and ATR from constrained 3D CSEM inversion at Gemini N.

data. The upper section may still be good reservoir, but with limited contribution to the CSEM response.

Predicting the well

We have now described two quantitative methods to predict hydrocarbon pay at Gemini N to integrate high-resolution seismic and CSEM with well calibration. One approach is an interpretation of high-resolution seismic inversion (P-Cable). This suggested a layered Stø Fm with ~12 m good reservoir below a thinner and higher AI upper section. The other approach is CSEM driven, using ATR from inversion and assuming a proper selection of a most feasible rock physics model from the Wisting well database. This came back with 11 m high-saturation hydrocarbon reservoir of high quality. The corroboration of the two approaches emphasizes the strength of joint quantitative interpretation in reservoir characterization. The results are in good alignment with the limited well information shared so far: The Gemini N well (7324/5-1) was drilled and encountered a 19 m gas column in the Stø formation in sandstone with good reservoir quality. The gas/water contact was not proven.

Conclusion

We describe application of CSEM interpretation concepts from Granli et al. (2017) to the Gemini N exploration target ~30 km to the northeast of Wisting. As summarized in Figure 1, only coinciding seismic DHI and CSEM high-resistivity isolate hydrocarbon scenarios. However, Gemini N has a weak CSEM anomaly compared to Wisting. A high-resolution 3D CSEM survey design was developed and has provided very accurate resistor (hydrocarbon saturated reservoir) characteristics. When integrated with high resolution P-Cable seismic during interpretation these new CSEM data lead to convincing quantitative predictions with application to detailed reservoir characterization.

Acknowledgement

We thank OMV Norge and EMGS for permission to publish this information, and TGS for permission to share their multi-client seismic data.

10.1190/segam2018-2995351.1

REFERENCES

Alvarez, P., A. Alvarez, L. Macgregor, F. Bolivar, R. Keirstead, and T. Martin, 2017, Reservoir properties integrating controlled-source electromagnetic, prestack seismic and well log data using a rock-physics framework: Case study in the hoop Area, Barents Sea, Norway: Interpretation, **5**, no. 2, SE43–SE60, https://doi.org/10.1190/INT-2016-0097.1.

Garden, M., O. Michot, M. Terenzoni, H. Hafslund Veire, J. R. Granli, L. M. Moskvil, K. Krathus-Larsen, 2017, Resolution, resolution, resolution - an ultra-high resolution seismic case study from the Barents Sea: 79th Annual International Conference and Exhibition, EAGE, Extended Abstracts, https://doi.org/10.3997/2214-4609.201701138.

Granli, J. R., H. Hafslund Veire, P. Gabrielsen, and J. P. Morten, 2017, Maturing broadband 3D CSEM for improved reservoir property prediction in the Realgrunnen Group at Wisting, Barents Sea: 87th Annual International Meeting, SEG, Expanded Abstracts, 2205–2209, https://doi.org/10.1190/segam2017-17727091.1.

Miotti, F., I. Guerra, F. Ceci, A. Lovatini, M. Paydayesh, M. Leathard, and A. Sharma, 2013, Petrophysical Joint Inversion of seismic and EM attributes: A case study: 83rd Annual International Meeting, SEG, Expanded Abstracts, 2516–2521, https://doi.org/10.1190/segam2013-0877.1.

Morten, J. P., H. Hafslund Veire, J. R. Granli, and P. T. Gabrielsen, 2017, Quantitative comparison of deep-reading well resistivity to 3D CSEM at Wisting: 87th Annual International Meeting, SEG, Expanded Abstracts, 1174–1178, https://doi.org/10.1190/segam2017-17723740.1.

Moskvil, L.M., H. Hafslund Veire, E. Stueland, J. R. Granli, K. Krathus-Larsen, O. Michot, 2018, High resolution seismic interpretation at Wisting: A breakthrough for shallow reservoir development, NPF Biennal Geophysical Seminar.